Enhanced DC-link voltage utilization for sliding mode controlled PMSM drives

Víctor Repecho, Andrés Sierra-González, Edorta Ibarra, Domingo Biel and Antoni Arias

***Abstract*—Sliding mode control (SMC) can be considered for torque regulation of permanent magnet synchronous machines (PMSM) when fast transient response and/or robustness under parameter uncertainties are required. In some particular applications, a voltage harmonic injection technique that enhances the DC-link voltage utilization should be incorporated into the controller to operate at high speeds. Although this is straightforward for pulse width modulated (PWM) drives, a convenient definition of the sliding surfaces and an appropriate injection procedure must be implemented when using SMC. In this work, a novel approach to generate zero sequence voltage harmonic injection in surface mounted (SM) PMSM drives controlled by a fixed switching frequency first order SMC is proposed. A theoretical analysis is provided verifying the sliding mode existence and demonstrating the system stability when the sliding mode is reached. Finally, experimentation is carried out in an off-the-shelf PMSM drive, where two voltage injection patterns are tested. In both cases, the DC-link voltage utilization is extended by a 15 %, confirming the validity of the proposal.**

***Index Terms*—Maximum DC-link voltage utilization, zero sequence third harmonic injection, SMC, PMSM.**

I. Introduction

Sliding Mode Control (SMC) features robustness against plant parameter variations and uncertainties while providing fast transient response [1]–[7]. Nevertheless, professional field engineers working on Permanent Magnet Synchronous Machine (PMSM) are generally reluctant to use SMC for torque/current controllers due to the lack of application notes and the supposed mathematical complexity of its analysis.

Several of the inherent SMC drawbacks, such as the variable switching frequency and the challenging (or difficult) digital implementation, have been lately addressed in the scientific literature [8]–[12] and successfully overcome. However, in the PMSM drive field, another relevant practical feature is the voltage harmonics injection, which up to date has not been sufficiently investigated. Such injection is required in applications where full DC-link voltage utilization is needed to achieve high mechanical speeds while postponing or eventually avoiding field weakening operation. This is not only desirable for general purpose electric drives [13], but also for state of the art applications such as battery powered electric vehicles [14]–[20] and electromechanical actuators [21]–[24], among others.

In PWM operated three-phase electric drives, full DC-link voltage utilization can be achieved by means of (i) directly injecting the harmonic signal v_n^* to the fundamental reference voltages [25]–[27], or (ii) by using space vector modulation (SVM), where signal injection is inherent to the modulation process [26], [28], [29]. Both techniques add to the fundamental reference voltage a zero sequence signal (3rd, 9th, 15th... harmonics) to increase the maximum amplitude of the output voltage by a factor of $2/\sqrt{3}$ without over-modulation [26], [30]. On the other hand, fundamental reference voltages are not present in SMC, since the controllers directly generate the discontinuous control signals. Therefore, the voltage injection signals should be included in the SMC design stage through the suitable definition of the sliding surfaces and their reference values. Among the few works that deal with the voltage harmonic injection in SMC, the neutral voltage v_n is controlled in [31] to introduce a third harmonic voltage component in a photovoltaic inverter. A phase voltage of the grid is sensed and combined with an Extended Kalman Filter (EKF) to provide v_n^*. Similarly, third harmonic injection is conducted in [32] by using an EKF for a grid connected voltage source inverter including an LCL filter. Both approaches determine v_n^* from the desired steady-state regime of the inverter, which depends on the inverter parameters, the DC-link voltage and the delivered power. As a consequence, these methods are not robust in the face of system variations. Moreover, the EKF includes additional dynamics to the system that may complicate the controller design.

In this work, a novel approach to generate voltage harmonic injection in a surface mounted (SM) PMSM drive controlled by a fixed switching frequency first order SMC is presented. The reference voltage v_n^* is calculated by only processing in real-time the equivalent control signals of the SMC. Since none of the PMSM parameters or measurements (motor currents, speed or position) have been used in the injection scheme, a robust operation is obtained. Thanks to this approach, it may be emulated any injection pattern existing in PWM controlled PMSM drives. The paper also presents a theoretical analysis verifying that a stable sliding mode exists with the new designed control scheme. Moreover, digital implementation details of the proposal in a widely used microcontroller are given, demonstrating its suitability for

This work was partially supported by the Government of Spain through the *Agencia Estatal de Investigación* Project DPI2017-85404-P, the *Generalitat de Catalunya* through the Project 2017 SGR 872, by the European Commission within the EU H2020 project FITGEN (grant agreement 824335), and by the Government of the Basque Country within the fund for research groups of the Basque University system IT978-16 and within the research program ELKARTEK as the project ENSOL2 (KK-2020/00077).

V. Repecho, D. Biel and A. Arias are with the Institute of Industrial and Control Engineering, Universitat Politècnica de Catalunya, Barcelona, Spain. A.Sierra-González is with Tecnalia Research and Innovation, Derio, Spain. E. Ibarra is with the Department of Electronic Technology, University of Basque Country (UPV/EHU) Bilbao, Spain. (mails:victor.repecho.del@upc.edu, andres.sierra@tecnalia.com, edorta.ibarra@ehu.es, domingo.biel@upc.edu, antoni.arias@upc.edu)

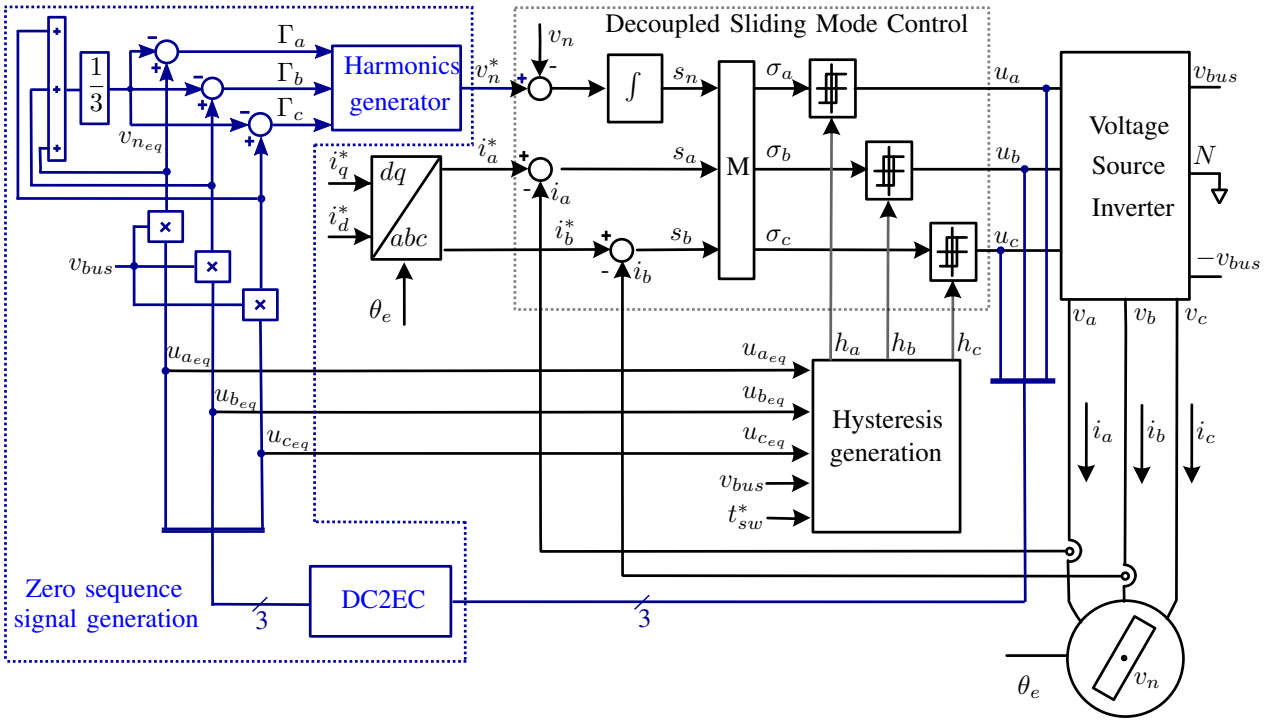

Fig. 1: Control scheme of the proposed SMC with enhanced DC-link voltage utilization.

industrial applications. Finally, experimental results in an off-the-self PMSM drive are provided under two different injection patterns.

II. Sliding mode control of SM-PMSMs with enhanced DC-link voltage utilization

Figure 1 shows the general diagram of the fixed switching frequency SMC [12] with the proposed zero sequence signal generation algorithm (in blue). In the following, an introduction to the decoupled SMC for PMSMs is presented and the zero sequence signal generation structure is detailed.

A. SM-PMSM model in the stationary reference frame

The stator voltage equations of an SM-PMSM in the stationary reference frame (*abc*) are given by [33]:

$$\mathbf{L}\frac{d\mathbf{i}}{dt} = -R\,\mathbf{i} - \mathbf{e}(\omega_e) + v_{bus}\mathbf{L}\mathbf{B}\,\mathbf{u}, \tag{1}$$

where $\mathbf{i} = [i_a, i_b, i_c]^T$, $\mathbf{u} = [u_a, u_b, u_c]^T$ and $\mathbf{e}(\omega_e) = [e_a, e_b, e_c]^T$ are the stator currents, control signals and back-EMF voltages, respectively. The signals u_a, u_b, u_c, which control the state of the VSI switches, can only take discrete values (1 or -1), and, in general, the back-EMF has a sinusoidal distribution in a three-phase SM-PMSM. Moreover, considering a star connection and a symmetric machine, the inductance matrix $\mathbf{L}$ is:

$$\mathbf{L} = \begin{bmatrix} L_a & 0 & 0 \\ 0 & L_b & 0 \\ 0 & 0 & L_c \end{bmatrix}, \tag{2}$$

and the matrix $\mathbf{B}$ becomes:

$$\mathbf{B} = \frac{1}{L_T}\begin{bmatrix} L_b + L_c & -L_c & -L_b \\ -L_c & L_a + L_c & -L_a \\ -L_b & -L_a & L_a + L_b \end{bmatrix}, \tag{3}$$

where $L_T = L_bL_c + L_aL_c + L_aL_b$.

B. Decoupled SMC

The SMC design steps detailed in [12] have been followed in this work. In order to carry out a decoupled sliding mode current control, at first the sliding surface matrix $\mathbf{S}$ that will guarantee zero tracking error must be selected [1]. As in a star connected motor only two of the three currents are linearly independent, only the control of two currents is necessary. Thus, the remaining degree of freedom can be effectively used to control the average value of the voltage v_n and improve the utilization of the DC-link voltage. Therefore, the switching functions are defined as:

$$\mathbf{S} = \left[i_a^* - i_a,\ i_b^* - i_b,\ \int (v_n^* - v_n)\,dt \right]^T. \tag{4}$$

In order to design the control laws guaranteeing asymptotic convergence to the desired steady-state, that is the derivative of a candidate Lyapunov function ($V = 0.5\boldsymbol{\sigma}^T\boldsymbol{\sigma}$) is negative, a new set of sliding surfaces $\boldsymbol{\sigma} = \mathbf{MS}$ are defined. The matrix $\mathbf{M}$ (Figure 1) that ensures the control decoupling [12], results in:

$$\mathbf{M} = \begin{bmatrix} L_a & 0 & 1 \\ 0 & L_b & 1 \\ -L_c & -L_c & 1 \end{bmatrix}. \tag{5}$$

With respect to the system behaviour under sliding motion, it is clear from (4) that once the sliding surfaces are reached

(and the sliding existence conditions are fulfilled, see section III-A) the currents and the average value of the voltage v_n track their reference signals and therefore the stability is guaranteed.

C. Variable Hysteresis Generator

The following control law assures convergence to a vicinity of a switching surface $\sigma_x = 0$:

$$u_x = \begin{cases} -1 & \text{if} \quad \sigma_x < -h_x, \\ 1 & \text{if} \quad \sigma_x > h_x, \end{cases} \tag{6}$$

where $x \in \{a, b, c\}$ and h_x is the hysteresis band of each controller. The hysteresis band generator (Figure 1) properly regulates the hysteresis bands of the comparators to achieve fixed switching frequency operation. The switching frequency should be high enough with respect to the system dynamics to guarantee that the switching function describes a piecewise linear behaviour. Thus, the control signal commutates at fixed switching frequency and the low frequency component of the dynamics and the steady-state operation of the drive are given by the ideal sliding motion. Moreover, as expected, it can be easily proved that the hysteresis band providing fixed switching frequency is highly dependent on the machine variables and parameters. In [12] this problem was overcome averaging the control signals and using the equivalent control signals [1] in the hysteresis band generator. As a result, the fixed switching frequency regulation becomes robust with respect to the PMSM parameter variations and to the harmonic injection.

D. Zero sequence signal generation under sliding mode

In PWM operated PMSM drives, the triplen harmonic signal is generated using the sinusoidal reference voltages v_a, v_b and v_c. The SMC does not generate such voltages, since directly provides discontinuous control signals to the inverter. In this work, the equivalent controls extracted from the system will be used for generating v_n^*, as depicted in blue in Figure 1.

From the SMC theory [1], the equivalent controls can be analytically determined by applying $\boldsymbol{\sigma} = 0$ and $\dot{\boldsymbol{\sigma}} = 0$. Hence, using $\mathbf{M}\dot{\mathbf{S}} = 0$, and replacing (1)-(5), the following is obtained:

$$u_{xeq} = \frac{1}{v_{bus}}(L_x \dot{i}_x^* + R i_x^* + e_x + v_n^*), \tag{7}$$

Knowing that when the neutral point is regulated to zero ($v_n^* = 0$), the equivalent control is sinusoidal, and the fundamental harmonic of the control can be identified in (7) as:

$$\Gamma_x = v_{bus} u_{xeq} - v_n^*. \tag{8}$$

When the reference v_n^* is not zero, the equivalent controls are no longer purely sinusoidal, since v_n tracks v_n^* in average under sliding motion, see (4). However, the injection algorithm needs three purely sinusoidal waveforms to properly generate the zero sequence signals. Therefore, when $v_n^* \neq 0$, it is necessary to recover the Γ_x signals and use them for the zero sequence generation (Figure 1). Note that Γ_x could be determined from (8), but this procedure needs to know v_n^*, which in turn is the output of the injection algorithm. To overcome this problem, the Γ_x signals are calculated using the following expression:

$$\Gamma_x = v_{bus} u_{xeq} - v_{n_{eq}}, \tag{9}$$

which corresponds to (8), but replacing v_n^* by $v_{n_{eq}}$, which is the averaged value of v_n. Knowing that the stator windings are sinusoidally distributed along the stator, v_n can be calculated as:

$$v_n = \frac{v_{bus}}{3}\left(u_a + u_b + u_c\right), \tag{10}$$

which is inherently discontinuous. Therefore, the averaged value of v_n can be approximated as

$$v_{n_{eq}} = \frac{v_{bus}}{3}\left(u_{a_{eq}} + u_{b_{eq}} + u_{c_{eq}}\right). \tag{11}$$

According to [1], the equivalent controls of (9) can be determined by averaging the corresponding discontinuous control signals (DC2EC block, Figure 1, see Section IV-A for further details).

Summarizing, in the scheme used to generate the reference signal v_n^* (Figure 1), the equivalent controls and $v_{n_{eq}}$ are firstly obtained from the control signals. Subsequently, the Γ_x signals are derived applying (9) and, finally, measuring the bus voltage value, the reference signal v_n^* is calculated either by applying the well-known $min - max$ technique or by any other zero sequence pattern.

Remark 1. *It has to be noted that the equivalent control is measured online under sliding motion and does not need the knowledge of the PMSM parameters or the machine state. As a conclusion, the proposed method, which only should measure the DC-link voltage, is robust with respect to the PMSM variables and parameters. This fact constitutes the main difference with respect to the approaches presented in [31] and [32].*

III. Impact of the zero sequence signal generation in the sliding mode

As it was previously pointed out in (7), the equivalent control is affected by the injected signal v_n^*. As a consequence, the sliding domain and the hysteresis of the comparators which ensure fixed switching frequency operation are also modified. Thus, this section is devoted to analyse the impact of the zero sequence signal generation to the sliding mode.

A. Sliding domain and DC-link voltage utilization

Sliding mode is ensured when the equivalent control behaves between the minimum and the maximum of the applied control signal, hence the expression $-1 < u_{xeq} < 1$ should be fulfilled for $x \in \{a, b, c\}$. Recalling (8), the sliding mode existence requires that the inequalities

$$-v_{bus} < \Gamma_x + v_n^* < v_{bus} \tag{12}$$

should be verified. Let us study the case for phase a. Once the sliding motion is reached, the inverter currents will perfectly track the sinusoidal references, i.e.

$$i_a^* = I \sin(\omega_e t), \tag{13}$$

where amplitude I will depend on PMSM desired speed and load conditions. Moreover, the back-EMF can also be considered sinusoidal:

$$e_a = \omega_e \psi_m \sin(\omega_e t), \tag{14}$$

where ω_e and ψ_m are the electrical angular speed and the permanent magnet flux linkage, respectively. Therefore, from (7) and (8), the fundamental harmonic is given by:

$$\Gamma_a = \Delta_a \sin(\omega_e t + \theta_a), \tag{15}$$

where

$$\Delta_a = \sqrt{(L_a I \omega_e)^2 + (RI + \omega_e \psi_m)^2}, \tag{16}$$

$$\theta_a = \arctan[L_a I \omega_e / (RI + \omega_e \psi_m)]. \tag{17}$$

When there is no DC-link voltage enhancement ($v_n^* = 0$), (12) results in $v_{bus} > \Delta_a$. Hence, the bus voltage is selected to fulfil this last inequality.

When the neutral voltage tracks a reference signal delivered by the Harmonic generator block, (12) can be rewritten as:

$$v_{bus} > \Delta_a \mid \sin(\omega_e t + \theta_a) + \frac{1}{6}\sin(3\omega_e t + 3\theta_a) \mid . \tag{18}$$

Finally, recalling that the maximum of the signal $\sin(\omega_e t + \theta_a) + \frac{1}{6}\sin(3\omega_e t + 3\theta_a)$ is 0.866, one can confirm that the DC-link usage is extended a 15.47%. Note that equivalent expressions are obtained for phases b and c.

Remark 2. *The previous analysis considers a reference signal with third harmonic. When the $min - max$ technique is applied, v_n^* not only has the third harmonic but also other triplen harmonics. In [34] it is proved that those triplen harmonics are eliminated in the line-to-line voltage waveforms and do not have any influence in the DC-link usage enhancement.*

B. Fixed switching frequency operation

The hysteresis generation block of Figure 1 fixes the switching period t_{sw}^* by adjusting the hysteresis bands h_x as a function of the equivalent controls [12]:

$$h_x = 0.25 t_{sw}^* v_{bus}(1 - u_{xeq}^2). \tag{19}$$

In Figure 2a the equivalent controls are plotted considering $\omega_m = 2500\pi/30$ rad/s and the PMSM parameters shown in Table I. The perfect sinusoidal waveform (in blue) is obtained when no injection is applied, while the one in black is obtained with injection. This confirms the aforementioned increment of $2/\sqrt{3}$ on the DC-link usage. Moreover, recalling that the equivalent control is a signal with a fundamental harmonic and its triplens, the hysteresis is also a periodic signal with

$$h_{max} = 0.25 t_{sw}^* v_{bus}, \tag{20}$$

$$h_{min} = 0.25 t_{sw}^* v_{bus}(1 - |u_{xeq}|_{max}^2). \tag{21}$$

Note that only h_{min} is affected by third harmonic injection (Figure 2b). Since the maximum value of the equivalent control is $|u_{xeq}|_{max} = \Delta_x / v_{bus}$ when there is no injection and is $|u_{xeq}|_{max} = 0.866\Delta_x / v_{bus}$ when the third harmonic is injected, the following relation is fulfilled:

$$\frac{h_{min-no}}{h_{min-third}} = \frac{v_{bus}^2 - \Delta_x^2}{v_{bus}^2 - (0.866\Delta_x)^2}, \tag{22}$$

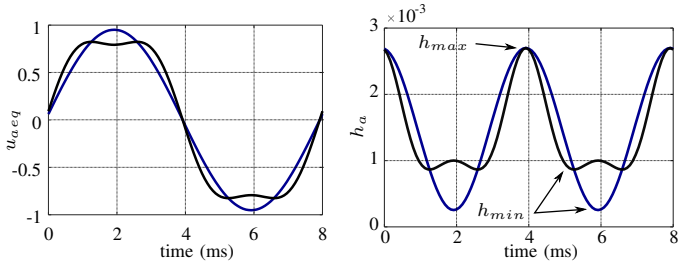

Fig. 2: (a) Equivalent control waveforms and (b) hysteresis bands evolution for a single period in the PMSM (Table I) for steady-state conditions at $\omega_m = 2500\pi/30$ rad/s, without (blue) and with (black) injection.

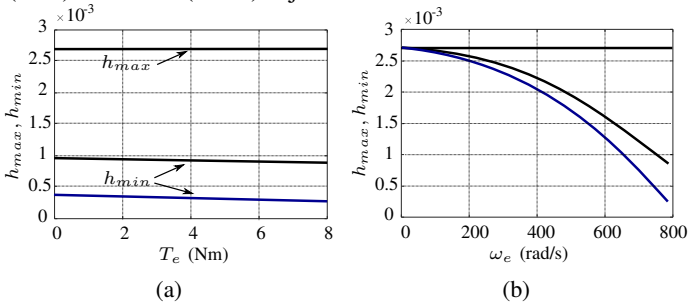

Fig. 3: Evolution of the maximum and minimum values of the hysteresis bands without (blue) and with (black) injection for (a) load and (b) speed variations.

where h_{min-no} and $h_{min-third}$ are the minimum values of the hysteresis for no injection operation and when the third harmonic is injected, respectively. From (22) it can be inferred that $h_{min-third} > h_{min-no}$ and it can be concluded that the signal injection not only does not make the switching frequency regulation worse but also reduces the hysteresis variation required to set it. Therefore, the injection of the third harmonic helps to reduce the total excursion of the required hysteresis value as Figure 2b depicts.

On the other hand, the load torque also varies the equivalent controls since it affects the amplitude I on (16). Nevertheless, the impact of the load torque in the equivalent control and in the hysteresis bands is low, since the EMF terms in (16) dominates the ones with I. Figure 3a shows how h_{max} is constant while h_{min} is almost unaffected by load conditions in both non-injection and injection scenarios. Finally, Figure 3b illustrates the strong speed dependence of the minimum hysteresis band (h_{min}). As the speed increases, the h_{min} decreases and eventually it might take the value zero which means that the DC bus limit is achieved.

IV. Experimental validation

Figure 4 shows the experimental platform used to test the control proposal. A 3-phase Unimotor 115E2 SM-PMSM fed by an Infineon FS50R06W1E3 VSI has been mounted. Table I summarizes the most significant parameters of the PMSM drive and the IP controller designed to regulate the machine mechanical speed. A DC-link voltage of 270 V has been considered as in a real EMA application [35].

TABLE I: PMSM drive parameters.

Parameter	Symbol	Value
Power, Torque, Speed	P, T_e, w_m	2.54 kW, 8.1 Nm, 3000 rpm
Motor Constants	K_T, K_e	0.93 Nm/A, 57 $V/krpm$
Pole pairs	p	3
Stator Inductances	L_a, L_b, L_c	1.5 $mH \pm 0.25\ mH$
Stator Resistance	R	0.36 Ω
Moment of Inertia	J	$4.57 \cdot 10^{-3}\ kgm^2$
Friction Coefficient	B	$8.75 \cdot 10^{-3}\ Nms$
Bus Voltage	$2v_{bus}$	270 V
Switching frequency	f_{sw}	12.5 kHz
IP Speed controller		
Sampling Period	T_{zw}	125 μs
Settling time at 2 %	ST_2	1 s
Damping factor	ζ	0.707
$k_i = 4.22^2 \cdot J/(\zeta^2 \cdot ST_2^2)$; $k_p = 2 \cdot 4.22 \cdot J/ST_2 - B$		

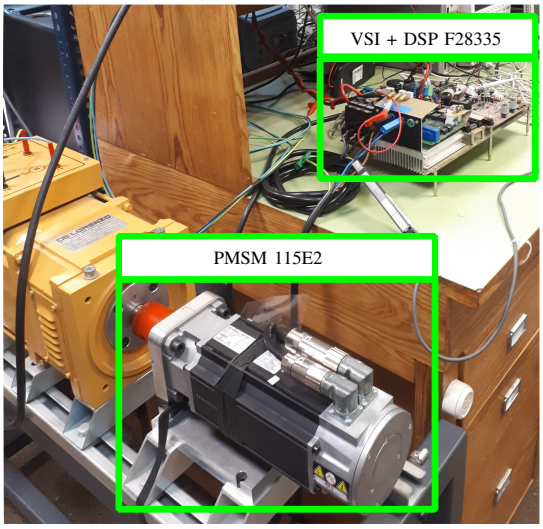

Fig. 4: Workbench with an off the shelf 3-phase Unimotor 115E2 SM-PMSM mechanically coupled with a loading DC machine, the micro-controller and VSI.

A. Digital implementation details

The control algorithm described in section II has been implemented in a Texas Instruments F28335 microcontroller. A predictive algorithm [12] has been used for the continuous time emulation of the hysteresis comparators. Thanks to this, with a sampling period of 5 μs the SMC behaves close to the ideal dynamics. The rest of the algorithm has been discretized using a standard procedure with a sampling period low enough with respect to the mechanical time constant. Therefore, the control has been implemented in two routines, one for SMC including the prediction algorithm and sampled at 5 μs and the mechanical speed control routine executed at 125 μs. This last routine also generates the variable hysteresis band. The SMC control task was executed with high priority and cannot be interrupted. The speed control code (which includes the v_n^* generation) is executed with low priority (so it can be continuously suspended by the SMC). In discrete time implementations, it is important to evaluate the resources used by digital devices [36], [37]. In this case, the CPU usage is around 84 %, which implies a high but safe utilization rate guaranteeing a correct execution.

For the derivation of the equivalent controls $u_{a_{eq}}$, $u_{b_{eq}}$ and $u_{c_{eq}}$, instead of using digital low pass filters which add delays to the measurements, an alternative method has been applied to the Discontinuous Controls to extract their Equivalent Controls (DC2EC block, Figure 1.) Three timers of the micro controller are programmed to measure the t_{on} and the switching period t_{sw} of the control signals. With these measurements, the equivalent control is approximated as follows:

$$u_{x_{eq}k} = 2\,\frac{t_{x_{on}k}}{t_{x_{sw}k}} - 1, \tag{23}$$

where k is the rising edge event of the corresponding control action. At any new $t_{x_{sw}k}$ measurement, a code is executed estimating the equivalent controls using (23) and updating the value of v_n^* according to the scheme shown in Figure 1 (blue part).

B. Experimental tests

Two experimental tests have been performed to validate the proposal.

1) Zero sequence generation at constant speed: In this particular test, voltage injection is carried out while operating at steady-state at 2500 rpm, close to the base speed. Two voltage harmonic patterns have been applied to show the flexibility of the proposal:

(a) The well-known $min - max$ technique [26].
(b) Third harmonic signal with variable gain, generated by performing the following expression:

$$v_n^* = \frac{2}{3v_{bus}^2}\Gamma_a\Gamma_b\Gamma_c = \frac{\Delta^3}{6\,v_{bus}^2}\sin(3\omega t + 3\theta), \tag{24}$$

which is not only extremely simple, but also automatically adapts its amplitude when Δ increases, see (16).

Figures 5, 6 and 7 show the test results: the motor voltage Γ_a (channel 2, yellow waveform), the $v_{n_{eq}}$ voltage (channel 4, blue waveform) measured through an analogue low pass filter with a cut-off frequency of 1 kHz, and, finally, the equivalent control voltage, $v_{bus}u_{a_{eq}}$ (channel 2, green signal) measured through the DAC LT2645 with the scale 2.5 V / 270 V.

From Figures 5 and 6 it can be validated that the proposed methodology works as expected. In both cases, the desired reduction of 15 % in the peak motor voltage is obtained when the injection is activated. Moreover, the expected behaviour of $v_{n_{eq}}$, triangular wave in Figure 5 and a purely sinusoidal in Figure 6, can also be confirmed.

Figure 7 illustrates the correct behaviour of the two previously mentioned signal injection techniques and, more importantly, validates the capability of harmonic injection with the proposed SMC supporting different injection techniques. It becomes clear that, when the method given by (24) is used, the same level of fundamental phase voltage reduction is achieved with a smaller injected signal.

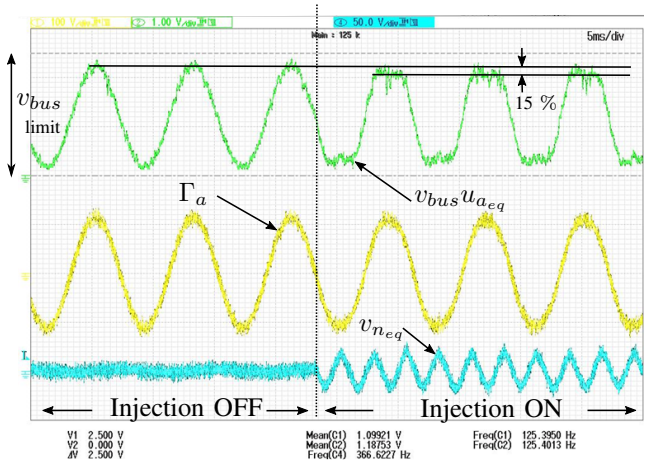

Fig. 5: Transient from no injection to $min - max$ signal injection. From top to bottom: equivalent voltage, $v_{bus}u_{a_{eq}}$, motor voltage, Γ_a, and averaged common voltage, $v_{n_{eq}}$.

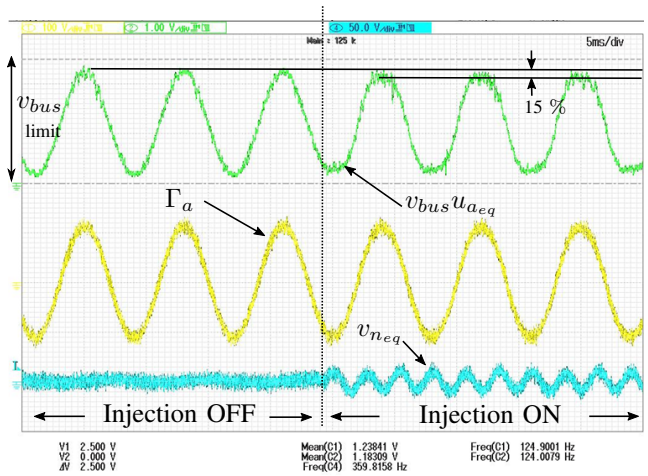

Fig. 6: Transient from no injection to variable gain third harmonic signal injection. From top to bottom: equivalent voltage, $v_{bus}u_{a_{eq}}$, motor voltage. Γ_a, and averaged common voltage, $v_{n_{eq}}$.

2) Zero sequence generation during speed reversal test: The second test is devoted to a speed reversal, and the results show the injection feature and confirm that the sliding motion is guaranteed at any time. Specifically, the motor varies its speed from 2500 rpm to -2500 rpm. Figures 8-11 show the following waveforms from the tests: the equivalent voltage of phase a, $v_{bus}u_{a_{eq}}$, measured through the DAC LT2645 scaled so $\pm$135 V correspond to 2.5 and 0 V, the equivalent common mode voltage $v_{n_{eq}}$ measured through an analogue low pass filter with a cut-off frequency of 1 kHz, the motor speed measured through the DAC LT2645, scaled so $\pm$3000 rpm correspond to 2.5 and 0 V, and the decoupled switching function σ_a measured through the DAC LT2645, scaled so its zero at 1.25 V.

Figures 8 and 10 present the speed reversal tests for both injection techniques while Figures 9 and 11 show zoomed views for more detail. The results validate the behaviour of both injections methods for all the electrical frequencies

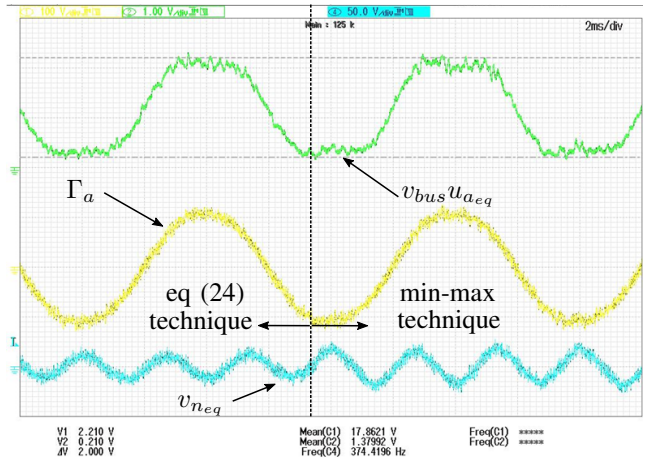

Fig. 7: Transient from zero sequence variable gain third harmonic to $min - max$. From top to bottom: equivalent voltage, $v_{bus}u_{a_{eq}}$, motor voltage, Γ_a, and averaged common voltage, $v_{n_{eq}}$.

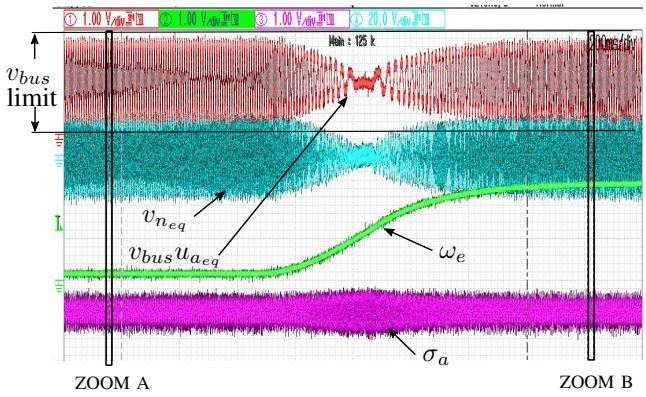

Fig. 8: Zero sequence min-max signal injection. From top to bottom: equivalent voltage, $v_{bus}u_{a_{eq}}$, averaged common voltage, $v_{n_{eq}}$, angular speed, ω_e, and switching function, σ_a.

involved during such a transient test. As it shows the behaviour of σ_a during the test, the control preserves the regulation property under the zero sequence injection, since the average value of σ is very close to 1.25 V, which corresponds to 0, thus confirming a perfect tracking of the reference current signals. It should be noticed how the hysteresis value is varied in order to bound the switching period of the control signals. This fact is confirmed from the switching function envelopes. With regard to the injection signals, again the triangular waveform (Figure 8) and the purely sinusoidal (Figure 10) can be observed. From the envelope of $v_{n_{eq}}$ is again validated that the variable gain methodology uses a lower reference voltage for the same bus utilization level.

V. Conclusion

This paper has demonstrated that SMC applied to PMSMs can exploit full DC-link voltage utilization as in PWM regulated drives naturally do with proper modulation techniques. Hence, it has been extensively justified the *virtual* increment, by a factor of $2/\sqrt{3}$, of the fundamental output voltages when

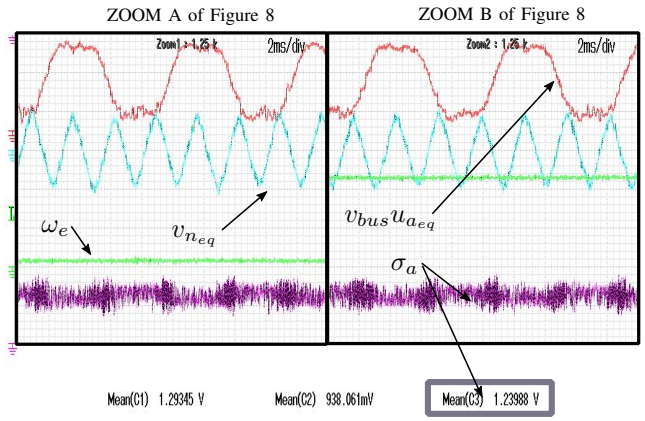

Fig. 9: Zoomed views of Figure 8. From top to bottom: equivalent voltage, $v_{bus}u_{a_{eq}}$, averaged common voltage, $v_{n_{eq}}$, angular speed, ω_e, and switching function, σ_a.

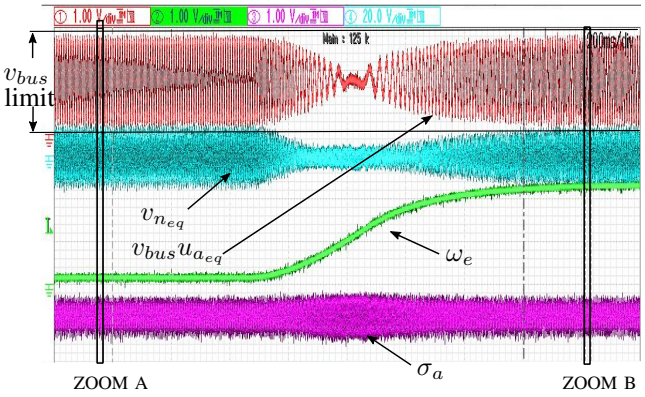

Fig. 10: Zero sequence variable gain signal injection. From top to bottom: equivalent voltage, $v_{bus}u_{a_{eq}}$, averaged common voltage, $v_{n_{eq}}$, angular speed, ω_e, and switching function, σ_a.

using SMC instead of space vector modulation or PWM with proper triplen harmonics addition. Therefore, SMC not only guarantees robustness and parameter independence, but also keeps the switching frequency constant and, with the contribution of this paper, establishes the methodology to inject any zero sequence voltages to maximise the DC-link voltage utilization, increasing by 15 % its base speed. Moreover, since none of the PMSM parameters nor any measured magnitudes (speed or position) have been used in the proposed structure, a robust injection harmonic has been obtained.

A rigorous SMC theoretical analysis verifying the sliding mode existence under the proposed harmonic injection conditions has been presented and the experimental results with an off-the-shelf PMSM demonstrates the utility of the proposal methodology, confirming that the injection voltage technique can operate with any zero sequence voltage. With such a wide harmonic injection capability, SMC can be further exploited for non-three-phase applications including multiphase power systems.

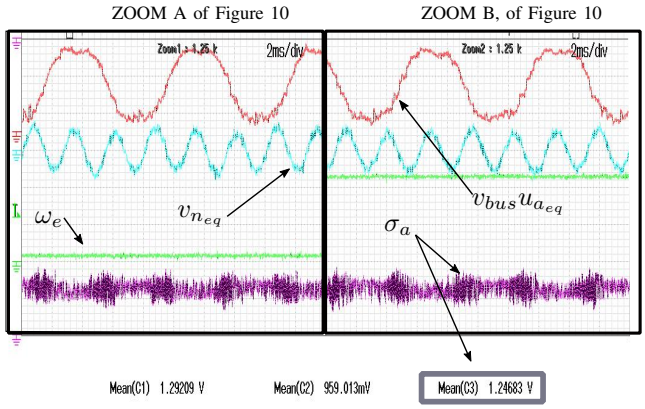

Fig. 11: Zoomed views of Figure 10. From top to bottom: equivalent voltage, $v_{bus}u_{a_{eq}}$, averaged common voltage, $v_{n_{eq}}$, angular speed, ω_e, and switching function, σ_a.

REFERENCES

[1] V. Utkin, J. Guldner, and J. Shi, *Sliding mode control in electro-mechanical systems*. CRC press, 2009, vol. 34.

[2] Q. Wang, H. Yu, M. Wang, and X. Qi, "An improved sliding mode control using disturbance torque observer for permanent magnet synchronous motor," *IEEE Access*, vol. 7, pp. 36 691–36 701, 2019.

[3] Y. Wang, Y. Feng, X. Zhang, and J. Liang, "A new reaching law for antidisturbance sliding-mode control of PMSM speed regulation system," *IEEE Transactions on Power Electronics*, 2019.

[4] K. Zhao, T. Yin, C. Zhang, J. He, X. Li, Y. Chen, R. Zhou, and A. Leng, "Robust model-free nonsingular terminal sliding mode control for PMSM demagnetization fault," *IEEE Access*, vol. 7, pp. 15 737–15 748, 2019.

[5] Y. Jiang, W. Xu, C. Mu, and Y. Liu, "Improved deadbeat predictive current control combined sliding mode strategy for PMSM drive system," *IEEE Transactions on Vehicular Technology*, vol. 67, no. 1, pp. 251–263, 2017.

[6] J. Liu, H. Li, and Y. Deng, "Torque ripple minimization of PMSM based on robust ILC via adaptive sliding mode control," *IEEE Transactions on Power Electronics*, vol. 33, no. 4, pp. 3655–3671, 2017.

[7] X. Zhang, L. Sun, K. Zhao, and L. Sun, "Nonlinear speed control for PMSM system using sliding-mode control and disturbance compensation techniques," *IEEE Transactions on Power Electronics*, vol. 28, no. 3, pp. 1358–1365, 2012.

[8] K. Jezernik, J. Korelič, and R. Horvat, "PMSM sliding mode FPGA-based control for torque ripple reduction," *IEEE Transactions on Power Electronics*, vol. 28, no. 7, pp. 3549–3556, 2012.

[9] S.-C. Tan, Y.-M. Lai, and C. K. Tse, "A unified approach to the design of PWM-based sliding-mode voltage controllers for basic DC-DC converters in continuous conduction mode," *IEEE Transactions on Circuits and Systems I: Regular Papers*, vol. 53, no. 8, pp. 1816–1827, 2006.

[10] E. Vidal-Idiarte, A. Marcos-Pastor, R. Giral, J. Calvente, and L. Martinez-Salamero, "Direct digital design of a sliding mode-based control of a PWM synchronous buck converter," *IET Power Electronics*, vol. 10, no. 13, pp. 1714–1720, 2017.

[11] E. Vidal-Idiarte, A. Marcos-Pastor, G. Garcia, A. Cid-Pastor, and L. Martinez-Salamero, "Discrete-time sliding-mode-based digital pulse width modulation control of a boost converter," *IET Power Electronics*, vol. 8, no. 5, pp. 708–714, 2015.

[12] V. Repecho, D. Biel, and A. Arias, "Fixed switching period discrete-time sliding mode current control of a PMSM," *IEEE Transactions on Industrial Electronics*, vol. 65, no. 3, pp. 2039–2048, 2018.

[13] A. Raghavendra and M. Mahesh, "Analysis of the energy and safety critical traction parameters for elevators," *EPE Journal*.

[14] Z. Zhang, R. Ma, L. Wang, and J. Zhang, "Novel PMSM control for anti-lock braking considering transmission properties of the electric vehicle," *IEEE Transactions on Vehicular Technology*, vol. 67, no. 11, pp. 10 378–10 386, 2018.

[15] F. Momen, K. Rahman, and Y. Son, "Electrical propulsion system design of Chevrolet Bolt battery electric vehicle," *IEEE Transactions on Industry Applications*, vol. 55, no. 1, pp. 376–384, 2019.

[16] L. Sepulchre, M. Fadel, M. Pietrzak-David, and G. Porte, "MTPV flux-weakening strategy for PMSM high speed drive," *IEEE Transactions on Industry Applications*, vol. 54, no. 6, pp. 6081–6089, 2018.

[17] J. Lara and A. Chandra, "Performance investigation of two novel HSFSI demodulation algorithms for encoderless FOC of PMSMs intended for EV propulsion," *IEEE Transactions on Industrial Electronics*, vol. 65, no. 2, pp. 1074–1083, 2018.
[18] M. Wang, C. Tong, Z. Song, J. Liu, and P. Zheng, "Performance analysis of an axial magnetic-field-modulated brushless double-rotor machine for hybrid electric vehicles," *IEEE Transactions on Industrial Electronics*, vol. 66, no. 1, pp. 806–817, 2019.
[19] A. Choudhury, P. Pillay, and S. S. Williamson, "DC-link voltage balancing for a three-level electric vehicle traction inverter using an innovative switching sequence control scheme," *IEEE Journal of Emerging and Selected Topics in Power Electronics*, vol. 2, no. 2, pp. 296–307, 2014.
[20] A. Battiston, J.-P. Martin, E.-H. Miliani, B. Nahid-Mobarakeh, S. Pierfederici, and F. Meibody-Tabar, "Comparison criteria for electric traction system using Z-source/quasi Z-source inverter and conventional architectures," *IEEE Journal of Emerging and Selected Topics in Power Electronics*, vol. 2, no. 3, pp. 467–476, 2014.
[21] T. Liu and M. Fadel, "An efficiency-optimal control method for mono-inverter dual-PMSM systems," *IEEE Transactions on Industry Applications*, vol. 54, no. 2, pp. 1737–1745, 2018.
[22] C. Sciascera, P. Giangrande, L. Papini, C. Gerada, and M. Galea, "Analytical thermal model for fast stator winding temperature prediction," *IEEE Transactions on Industrial Electronics*, vol. 64, no. 8, pp. 6116–6126, 2017.
[23] W. Cao, B. Mecrow, G. Atkinson, J. Bennett, and D. Atkinson, "Overview of electric motor technologies used for more electric aircraft (MEA)," *IEEE Transactions on Industrial Electronics*, vol. 59, no. 9, pp. 3523–3531, 2012.
[24] V. Madonna, P. Giangrande, L. Lusuardi, A. Cavallini, C. Gerada, and M. Galea, "Thermal overload and insulation aging of short duty cycle, aerospace motors," *IEEE Transactions on Industrial Electronics*, DOI: 10.1109/TIE.2019.2914630, 2019.
[25] D. G. Holmes and T. A. Lipo, *Modulation of Three Phase Voltage Source Inverters*. Wiley-IEEE Press, 2003, ch. 5, pp. 215–257.
[26] S. Kouro, J. Leon, L. Franquelo, J. Rodriguez, and B. Wu, *Power Electronics and Motor Drives: DC-AC converters*. CRC Press, 2016, ch. 14, pp. 1–49.
[27] R. Picas, J. Zaragoza, J. Pou, S. Ceballos, G. Konstantinou, and G. J. Capella, "Study and comparison of discontinuous modulation for modular multilevel converters in motor drive applications," *IEEE Transactions on Industrial Electronics*, vol. 66, no. 3, pp. 2376–2386, 2019.
[28] M. Priestley, J. E. Fletcher, and C. Tan, "Space-vector PWM technique for five-phase open-end winding PMSM drive operating in the overmodulation region," *IEEE Transactions on Industrial Electronics*, vol. 65, no. 9, pp. 6816–6827, 2018.
[29] S. Kim, "Chapter 7 - Pulse width modulation inverters," in *Electric Motor Control*, S.-H. Kim, Ed. Elsevier, 2017, pp. 265–340.
[30] T. Schoenen, A. Krings, D. van Treek, and R. De Doncker, "Maximum DC-link voltage utilization for optimal operation of IPMSM," in *Proc. of the IEEE International Electric Machines and Drives Conference*, 2009, pp. 1547–1550.
[31] E. Alarcon-Gallo, "Third harmonic injection on sliding mode control for a three-phase, three-wire inverter," in *Proc. of the Annual Conference of the IEEE Industrial Electronics Society (IECON)*, 2013, pp. 1910–1915.
[32] R. Guzman, L. Garcia de Vicuña, M. Castilla, J. Miret, and H. Martin, "Variable structure control in natural frame for three-phase grid-connected inverters with LCL filter," *IEEE Transactions on Power Electronics*, vol. 33, no. 5, pp. 4512–4522, 2018.
[33] P. C. Krause, O. Wasynczuk, S. D. Sudhoff, and S. Pekarek, *Analysis of electric machinery and drive systems*. Wiley-IEEE Press, 2013.
[34] J. A. Houldsworth and D. A. Grant, "The use of harmonic distortion to increase the output voltage of a three-phase PWM inverter," *IEEE Transactions on Industry Applications*, vol. IA-20, no. 5, pp. 1224–1228, 1984.
[35] F. Grumm, J. Storjohann, A. Lücken, M. F. Meyer, M. Schumann, and D. Schulz, "Robust primary protection device for weight-optimized pem fuel cell systems in high-voltage dc power systems of aircraft," *IEEE Transactions on Industrial Electronics*, vol. 66, no. 7, pp. 5748–5758, 2018.
[36] F. Naseri, Z. Kazemi, E. Farjah, and T. Ghanbari, "Fast detection and compensation of current transformer saturation using extended kalman filter," *IEEE Transactions on Power Delivery*, vol. 34, no. 3, pp. 1087–1097, 2019.
[37] F. Naseri, E. Farjah, T. Ghanbari, Z. Kazemi, E. Schaltz, and J. Schanen, "Online parameter estimation for supercapacitor state-of-energy and state-of-health determination in vehicular applications," *IEEE Transactions on Industrial Electronics*, vol. 67, no. 9, pp. 7963–7972, 2020.

Víctor Repecho received the B.S, M.S. and Ph.D. degrees in electronic engineering from the Universitat Politècnica de Catalunya (UPC), Barcelona, Spain, in 2006, 2012 and 2018, respectively. Since 2010, he has been a development Engineer with the Institute of Industrial and Control Engineering (IOC) and since 2019 he has been an Assistant Professor in the Automatic control Department, both at UPC. His research fields are related to digital control, nonlinear control, and control of power electronic converters.

Andrés Sierra-González received his B.S. degree in Electronics in 2008 from Andes University (Colombia) and an M.Eng. from the University of the Basque Country (Spain) in 2017. He is currently working toward the PhD degree in Electronics and Telecommunication at the University of the Basque Country. He worked as an Electronics Engineer in the mining and energy industry from 2009 to 2013. Next, he was a Research Assistant at Andes University from 2014 to 2016. Then, he worked as a researcher in the Energy Management division of IK4-IKERLAN in 2017. He is currently a Control Systems Researcher applied to electromobility applications at Tecnalia Research and Innovation (Spain).

Edorta Ibarra received the first M.Sc. degree in electronic engineering from the University of the Basque Country, Bilbao, Spain, in 2004, the second M.Sc. degree in electronic physics from the University of Cantabria, Santander, Spain, in 2005, and the Ph.D. degree in power electronics from the University of the Basque Country, in 2011. During 2006 to 2007, he was with the Technical Engineering School of Bilbao, Spain. From 2007 to 2014, he was with the Applied Electronic Research Group, University of the Basque Country. From 2014 to 2016, he was with Tecnalia Research & Innovation, Industry and Transport Unit, Derio, Spain. Since 2016, he has been an Assistant Professor in the Department of Electronic Technology, University of the Basque Country. His current research interests include power electronics and control for electromobility applications and particle accelerators.

Domingo Biel received the B.S, M.S. and Ph.D. degrees in telecommunications engineering from the Universitat Politècnica de Catalunya (UPC), Barcelona, Spain, in 1990, 1994 and 1999, respectively. Since 1998, he has been an Associate Professor in the Electronic Engineering Department, UPC, where he teaches power electronics and control theory. He is the coauthor of around 25 papers in international journals and more than 70 communications in international conferences. His research fields are related to nonlinear control and its application to renewable energy systems and power electronics.

Antoni Arias received the BEng degree in electrical engineering, MEng and PhD degrees in control and electronic engineering from the Universitat Politècnica de Catalunya (UPC), Catalonia, Spain, in 1993, 1997 and 2001 respectively. From 1992/95 he worked at a local industrial electronics company. Since 1996 he has been a Lecturer at the UPC and was appointed as an Associate Professor in 2002. In 2003/04 he joined as a Visiting Fellow the PEMC Group at the University of Nottingham, UK. In 2011/12 he was a MCF invité at the GeePs, France. His research interests include sensorless variable-speed drive systems, power electronics converters and control strategies.